Myocardial Loss of IRS1 and IRS2 Causes Heart Failure and Is Controlled by p38α MAPK During Insulin Resistance

Yajuan Qi,[1,2] Zihui Xu,[1,3] Qinglei Zhu,[1] Candice Thomas,[1] Rajesh Kumar,[1] Hao Feng,[1] David E. Dostal,[1] Morris F. White,[4] Kenneth M. Baker,[1] and Shaodong Guo[1]

Cardiac failure is a major cause of death in patients with type 2 diabetes, but the molecular mechanism that links diabetes to heart failure remains unclear. Insulin resistance is a hallmark of type 2 diabetes, and insulin receptor substrates 1 and 2 (IRS1 and IRS2) are the major insulin-signaling components regulating cellular metabolism and survival. To determine the role of IRS1 and IRS2 in the heart and examine whether hyperinsulinemia causes myocardial insulin resistance and cellular dysfunction via IRS1 and IRS2, we generated heart-specific IRS1 and IRS2 gene double-knockout (H-DKO) mice and liver-specific IRS1 and IRS2 double-knockout (L-DKO) mice. H-DKO mice had reduced ventricular mass; developed cardiac apoptosis, fibrosis, and failure; and showed diminished Akt→forkhead box class O-1 signaling that was accompanied by impaired cardiac metabolic gene expression and reduced ATP content. L-DKO mice had decreased cardiac IRS1 and IRS2 proteins and exhibited features of heart failure, with impaired cardiac energy metabolism gene expression and activation of p38α mitogen-activated protein kinase (p38). Using neonatal rat ventricular cardiomyocytes, we further found that chronic insulin exposure reduced IRS1 and IRS2 proteins and prevented insulin action through activation of p38, revealing a fundamental mechanism of cardiac dysfunction during insulin resistance and type 2 diabetes. *Diabetes* 62:3887–3900, 2013

Diabetes promotes cardiac failure and increases patient morbidity and mortality, with two-thirds of patients with type 2 diabetes dying of heart failure (1). In the patient population, 90–95% are type 2 patients with diabetes in whom insulin resistance is the primary contributor to metabolic and cardiac dysfunction (1). Intensive insulin therapy increases the risk of cardiovascular dysfunction and the death rate by twofold in patients with type 2 diabetes (Action to Control Cardiovascular Risk in Diabetes trial) (2). Thus, understanding the mechanisms responsible for insulin action, resistance, and related cardiac dysfunction will be critical for the development of new strategies for treatment of heart failure.

The heart is an insulin-responsive and energy consuming organ that requires a constant fuel supply to maintain intracellular ATP for myocardial contraction (3). Upon binding to the cell surface receptor, insulin activates its receptor tyrosine kinase, which phosphorylates and recruits insulin receptor (IR) substrates (IRS) 1 to 4 (IRS1, IRS4), and other scaffold proteins, including SHC, CBL, APS, SH2B, GAB1, and DOCK1, that trigger downstream signaling cascades, including phosphatidylinositide 3-kinase (PI-3K) and mitogen-activated protein kinases (MAPKs) (4–6). Activation of PI-3K generates phosphatidylinositol(3-5)-triphosphate (PIP3), recruiting the 3-phosphoinositide–dependent protein kinase-1 and -2 (PDK1 and PDK2) and Akt to the plasma membrane, where Akt is activated by PDK1-mediated phosphorylation at T^{308} and PDK2-mediated phosphorylation at S^{473} (7,8). Akt phosphorylates downstream targets, including inhibitors of macromolecular synthesis, such as glycogen synthase kinase-3β (Gsk3β, glycogen synthesis), tuberous sclerosis protein-2 (Tsc2), and p70S6K (protein synthesis), and forkhead transcription factor forkhead box class O1 (Foxo1) (gene transcription). Akt phosphorylates Foxo1 at S^{253} and inhibits transcriptional activity of Foxo1, which regulates a variety of physiological functions such as energy metabolism (9,10), myocardial growth (11–13), and survival (14). Thus, Akt→Foxo1 phosphorylation mediates the action of insulin and serves as an indicator of insulin sensitivity (5,15).

Systemic IRS1-null mice display growth retardation and develop peripheral insulin resistance mainly in skeletal muscle but not diabetes, owing to IRS2-depedent pancreatic β-cell growth and compensatory insulin secretion (16). Systemic IRS2-null mice display metabolic defects in liver, muscle, and adipose tissues but develop diabetes owing to pancreatic β-cell failure (17). We recently demonstrated that deletion of both IRS1 and IRS2 genes in the liver of L-DKO mice prevents activation of hepatic Akt→Foxo1 phosphorylation and results in the development of diabetes (5,18) and that deletion of both IRS1 and IRS2 in cardiac and skeletal muscle causes heart failure and death of animals at the age of 2 to 3 weeks (19). These results indicate that IRS1 and IRS2 are major mediators of insulin action to support physiological functions in many organs.

In this study, we deleted both IRS1 and IRS2 genes exclusively in the hearts of mice and determined cardiac function. We further examined the regulatory mechanisms for the myocardial loss of IRS1 and IRS2 in mouse models with insulin resistance. In particular, we tested the hypothesis that hyperinsulinemia—chronic or prolonged insulin exposure—can result in myocardial insulin resistance by suppressing IRS1 and IRS2.

RESEARCH DESIGN AND METHODS

Mice. Procedures used in animal experiments were approved by the Texas A&M Health Science Center Institutional Animal Care and Use Committee. The floxed IRS1 mice (IRS1$^{L/L}$), IRS2 mice (IRS2$^{L/L}$), albumin-Cre mice, and liver-specific IRS1 and IRS2 gene double-knockout (L-DKO) mice (albumin-Cre::IRS1$^{L/L}$::IRS2$^{L/L}$) have been previously described (5). MHC-Cre mice were purchased from The Jackson Laboratory (Bar Harbor, ME; stock #9074) to breed to IRS1$^{L/L}$::IRS2$^{L/L}$ mice, generating heart-specific IRS1 and IRS2 gene double-knockout (H-DKO) mice (MHC-Cre::IRS1$^{L/L}$::IRS2$^{L/L}$), H-DKO-het (MHC-Cre::IRS1$^{L/+}$::IRS2$^{L/+}$), and control littermates (IRS1$^{L/L}$::IRS2$^{L/L}$ mice). All mice were on a C57BL/6 and FVB129 Sv mixed background and fed a regular chow diet with 9% of energy derived from fat. The high-fat diet (HFD) consists of 45% calories from fat, 25.6% carbohydrate, and 16.4% protein (Research Diets, Inc., New Brunswick, NJ). C57BL/6 and *db/db* and mice were purchased from The Jackson Laboratory. Male mice and control littermates were used in all experiments.

Echocardiography. Echocardiograms were performed on anesthetized mice using a Visual Sonics Vevo 2100 system equipped with a 40-MHz linear probe, as previously described (12).

Blood biochemistry and metabolic analysis. Serum from mice fasted overnight were analyzed for insulin, triglycerides, and free cholesterol using commercial kits. Cardiac ATP concentrations were measured with an Enzylight ATP assay kit, as previously described (20).

Histological analysis. Hearts were fixed in 10% formaldehyde and stained with hematoxylin and eosin, Masson trichrome, and Oil Red O staining to visualize morphological features, fibrosis, and triglycerides, as previously described (10).

Apoptotic analysis. Hearts were fixed in 10% paraformaldehyde and embedded in paraffin. Paraffin-embedded sections (5 μm) were incubated at 60°C for 15 min, dewaxed, and rehydrated. Apoptosis was detected using the TUNEL assay (In situ Cell Death Detection Kit, Roche), according to the manufacturer's instructions.

Protein analysis and immunoblotting. The same amount of protein was resolved by SDS-PAGE and transferred to nitrocellulose membrane for Western blot. Signal intensity was measured and analyzed using ImageJ software (National Institutes of Health), as previously described (15).

Primary cardiomyocyte isolation and cell culture. Primary cultures of neonatal rat ventricular cardiomyocytes (NRVMs) were prepared from hearts of 1- to 2-day-old Sprague-Dawley rat pups, as previously described (21).

Adenovirus infection of cardiomyocytes. NRVMs were cultured in Dulbecco's modified Eagle's medium (DMEM)/M199 medium with serum for 48 h and then transfected by adding adenovirus expressing green fluorescent protein (GFP), IRS1, IRS2, GFP-fused wild-type p38 (p38-WT), and dominant-negative p38 (p38-DN). The dose of adenovirus is indicated as multiplicity of infection (MOI). Cells were infected with adenovirus for 8 h, and then fresh DMEM/M199 medium with serum was changed for another 8 h of culturing. Cells were serum-starved for 8 h before the insulin intervention. For MG132 treatment, the proteasome inhibitor was added to cells for 0.5 h before addition of adenovirus. After 8 h of adenovirus infection, cells were washed and fresh DMEM/M199 medium added for another 8 h of culturing before cellular protein lysates were prepared for immunoblotting.

RNA isolation and quantitative real-time PCR analysis. RNA was extracted with Trizol Reagent (Invitrogen), cDNA synthesis used the SuperScript first-strand synthesis system (Bio-Rad Laboratories, Inc.), and gene expression was measured with the SYBER Green Supermix system (Bio-Rad Laboratories, Inc.), as described previously (15). The PCR primers are listed in the Supplementary Methods.

Statistical analysis. Results are presented as the mean ± SEM. Data were analyzed by one-way and two-way ANOVA and the Turkey post hoc test to determine *P* values. *P* < 0.05 was considered statistically significant, as previously described (5).

RESULTS

Cardiac deletion of IRS1 and IRS2 prevents Akt→Foxo1 phosphorylation and causes cardiac dilation and heart failure in mice.

To assess the role of IRS1 and IRS2 in cardiac function, cellular signaling, and gene expression, we generated H-DKO mice specifically deficient in the IRS1 and IRS2 genes in the heart. In the H-DKO mice, IRS1 and IRS2 proteins were absent in the heart and normally expressed in the skeletal muscle, fat, and liver (Supplementary Fig. 1). Akt phosphorylation at T^{308} and S^{473}, indicative of PDK1 and PDK2 activation, respectively, and Akt-induced Foxo1 phosphorylation at S^{253} were completely blocked (Fig. 1A).

Phosphorylation of p70 ribosome S6 kinase (p70S6K), a target of mammalian target of rapamycin (mTOR) downstream from PI-3K for protein synthesis, was markedly reduced; however, extracellular signal–related kinase (ERK)1/2, p38, and Jun NH$_2$-terminal kinase (JNK) phosphorylation were unchanged in H-DKO hearts.

H-DKO mice died at the ages of 6 to 8 weeks, without a change in body weight (Fig. 1B and Table 1). In H-DKO hearts, cardiac left ventricular weight was reduced by 20% (*P* < 0.05; Table 1), and there was global chamber dilatation, with thinned cardiac muscle walls (Fig. 1C). Apoptotic cells were detected in H-DKO hearts but not in control hearts (Fig. 1D). Cardiomyocytes were irregularly arranged as revealed by hematoxylin and eosin staining (Fig. 1E), and interstitial fibrosis was notably increased (Fig. 1F). Systolic parameters for ejection fraction (EF) and fractional shortening (FS), as determined by echocardiography, were reduced by 70 and 60%, respectively, compared with the control (Fig. 1G). There was severe diastolic failure, as indicated by the mitral valve flow velocity (E-to-A ratio), which was not measurable because late (A′) filling waves were not detectable and early (E) filling waves were severely depressed. Isovolumic relaxation time and isovolumic contraction time could not be distinguished from aortic ejection time (Table 1). Cardiac ATP content was decreased by 40% (Fig. 1H).

Several metabolic parameters were measured in H-DKO mice at the age of 5 weeks. The blood glucose concentration was slightly reduced (H-DKO: 65 ± 6 mg/dL vs. control: 80 ± 7 mg/dL, *n* = 6 mice per group; *P* < 0.05) and serum triglycerides were increased by twofold (H-DKO: 130 ± 12 mg/dL vs. control: 60 ± 5 mg/dL, *n* = 6–10; *P* < 0.05). Serum insulin and free cholesterol were unchanged, and results of glucose and insulin tolerance tests in H-DKO mice were within normal reference ranges compared with control mice (data not shown).

Cardiac loss of IRS1 and IRS2 disrupts cardiac metabolic gene expression.

Compared with control, H-DKO hearts had increased expression of the heart failure marker genes ANP, BNP, and β-MHC, by 20-, 18-, and 40-fold, respectively (*P* < 0.05). Expression of the fibrosis marker gene TGF-β1 and collagen I was significantly increased by 2.5-fold each; however, expression levels of α-MHC, IRS1, and IRS2 were markedly reduced (Fig. 1I). We measured expression of genes that regulate glucose and lipid metabolism: H-DKO hearts exhibited reduced mRNA levels of the glucose transporter genes Glut1, Glut4, and glucokinase (GK) for glycolysis, by 50, 80, and 30%, respectively, compared with control (*P* < 0.05), and had an eightfold increase of pyruvate dehydrogenase kinase-4 (PDK4), a key enzyme and Foxo1 target gene (22), inhibiting glucose oxidation (*P* < 0.05; Fig. 1I). Lipid synthesis and oxidation genes were decreased in H-DKO hearts. For example, H-DKO hearts had marked reductions in the expression of genes encoding fatty acid synthase (Fasn), acetyl-CoA carboxylase (ACC1), very long-chain acyl-CoA dehydrogenase (VLCAD) for lipid metabolism, and peroxisome proliferator-activated receptor-γ coactivator 1α (PGC1α), which controls mitochondrial biogenesis and lipid oxidation (Fig. 1I). Expression of mitochondrial gene transcription factor (Tfam), a key nuclear gene controlling mitochondrial biosynthesis was significantly reduced by 50%, whereas expression of nuclear respiratory factor (NRF1) was unchanged. Moreover, the heme oxygenase-1 (Hmox-1) that catalyzes degradation of heme, a key component of mitochondria, was increased by sixfold (Fig. 1I),
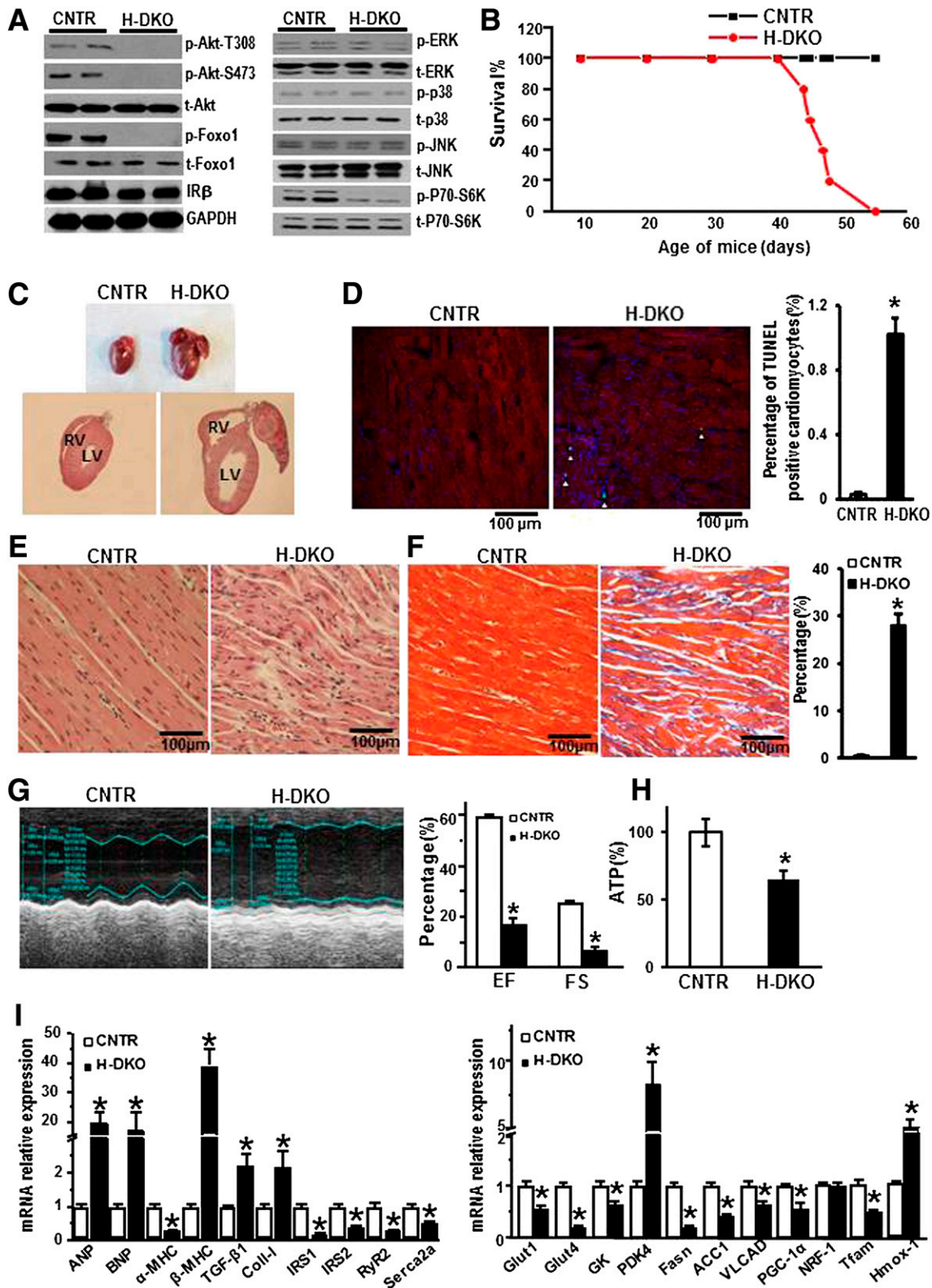
FIG. 1. Cardiac suppression of IRS1 and IRS2 diminishes Akt→Foxo1 phosphorylation, causes heart failure, and alters cardiac metabolic gene expression in mice H-DKO mice compared with control (CNTR) mice. *A*: Immunoblot detection for insulin-signaling molecules in the random-fed hearts of H-DKO and control mice at the age of 5 weeks (*n* = 2 mice per group). GAPDH, glyceraldehyde-3-phosphate dehydrogenase. *B*: Survival curve of H-DKO and control mice (*n* = 15 male mice per group). *C*: Cardiac morphology in ventricular chamber sections from the H-DKO and control mice at the age of 5 weeks. IVRT, isovolumic relaxation time; LV, left ventricle; RV, right ventricle. *D*: Apoptosis was detected using TUNEL assay. Actin filaments and nuclei of cardiac myocytes were counterstained using Alexa Fluor 546 phalloidin (Invitrogen) and DAPI, respectively. Positively stained nuclei were counted from 6–12 sections per heart and 3 hearts per treatment group. Apoptotic cells are green and indicated by triangles. Numbers of the apoptotic cells under 500 μm^2 of sections were counted and are shown as percentage. *$P < 0.05$ vs. control. *E*: Cardiac histology. Representative transverse section of left ventricle stained with hematoxylin and eosin (original magnification ×200). *F*: Cardiac interstitial fibrosis using Masson-Trichrome staining (original magnification ×200). Fibrotic zones were analyzed and are shown as percentage of the

TABLE 1
Echocardiographic parameters of H-DKO and L-DKO versus control mice

Variable	Control	H-DKO	Control	L-DKO
	5 weeks		24 weeks	
BW (g)	15.1 ± 1.2	13.2 ± 1.5	27.1 ± 2.5	26.10 ± 2.0
HVW (mg)	69.6 ± 4.1	54.9 ± 5.1*	119.9 ± 10.1	116.4 ± 11.6
HVW/BW (mg/g)	4.64 ± 0.11	4.17 ± 0.03*	4.4 ± 0.4	4.2 ± 0.4
HVW/TL (mg/mm)	43.2 ± 2.5	34.1 ± 3.2*	69.1 ± 8.6	67.2 ± 4.5
CO (mL/mm)	12.8 ± 0.8	5.7 ± 1.2*	21.9 ± 1.7	16.0 ± 0.6*
CI (L/min/m^2)	2.30 ± 0.14	1.12 ± 0.23*	2.66 ± 0.17	2.20 ± 0.08*
LVID-s (mm)	2.46 ± 0.05	3.86 ± 0.09*	2.65 ± 0.08	2.93 ± 0.11*
LVID-d (mm)	3.30 ± 0.03	4.15 ± 0.08*	3.74 ± 0.10	3.79 ± 0.11
MV Decl (ms)	—	—	26.71 ± 1.39	29.31 ± 2.29*
IVCT (ms)	—	—	18.43 ± 0.22	20.87 ± 0.56*
MV E-to-E′	—	—	37.00 ± 3.62	41.90 ± 3.46*
E′-to-A′	—	—	1.04 ± 0.04	0.76 ± 0.05*

BW, body weight; CI, cardiac index; CO, cardiac output; E′-to-A′, ratio of early diastolic peak (E′) velocity to late diastolic peak (A′) velocity; HVW, heart ventricle weight; IVCT, isovolumic contraction time; LVID-d, left ventricular internal dimension at diastole; LVID-s, left ventricular internal dimension at systole; MV Decl, mitral valve E wave deceleration time; MV E-to-E′, ratio of mitral valve peak early filling (E) velocity to early diastolic peak (E′) velocity; TL, tibial length. All measurements were from male mice. Values are the mean ± SEM (n = 4–10). *P < 0.05 vs. control mice.

suggesting mitochondrial dysfunction in H-DKO hearts. In addition, expression of ryanodine receptor 2 (RyR2) and sarcoplasmic reticulum ATPase (Serca2A), which govern calcium release and intake from the sarcomere to cytosol, were markedly decreased (Fig. 1*I*), indicating a calcium mishandling in H-DKO hearts. Taken together, H-DKO hearts disrupted the Akt→Foxo1 signaling cascade, markedly induced apoptosis, impaired metabolic, mitochondrial, and calcium-handling gene expression, and also decreased cardiac ATP production.

Cardiac loss of IRS1 and IRS2 protein and activation of p38 in HFD and *db/db* mice. To test the hypothesis that cardiac loss of IRS1 and IRS2 is involved in diabetes and/or insulin resistance, we determined protein levels of IRS1 and IRS2 in the hearts of HFD mice and *db/db* mice, which have been reported to have cardiac dysfunction (12,23). The HFD mice exhibited hyperinsulinemia after 4 months of HFD treatment, whereas *db/db* mice exhibited hyperinsulinemia and hyperglycemia, as we previously reported (5,10). IRS1 and IRS2 protein levels and Akt phosphorylation were reduced, whereas p38 phosphorylation was increased in the hearts of HFD and *db/db* mice, compared with control (Fig. 2*A* and Supplementary Fig. 2). Echocardiographic analysis indicated that the cardiac function was significantly impaired in HFD and *db/db* mice: EF and FS were reduced by 18 and 17%, respectively, in HFD-mice; EF and FS were reduced by 36 and 38% in *db/db* mice, respectively, compared with control (Fig. 2*A*).

Degradation of IRS1 and IRS2 diminishes AKT→Foxo1 phosphorylation and enhances p38 in L-DKO hearts. We further examined the cardiac signaling and function in another mouse model we recently developed—L-DKO mice (deficient in hepatic IRS1 and IRS2 genes), which developed insulin resistance and exhibited a reduction in serum triglycerides (L-DKO: 34.7 ± 2.9 mg/dL vs. control: 49.8 ± 4.8 mg/dL, n = 6; P < 0.05), distinct from the HFD and *db/db*

mice (5). L-DKO mice at the age of 6 months exhibited a 17-fold increase in the serum insulin level compared with control (L-DKO: 4.49 ± 0.26 ng/mL vs. control: 0.26 ± 0.03 ng/mL, n = 6; P < 0.05) but displayed a normal blood glucose concentration in the overnight fasting state (L-DKO: 67 ± 6.7 mg/dL vs. control: 61 ± 3 mg/dL, n = 6; P = 0.85). We examined phosphorylation/activation of Akt and MAP kinases in the heart of these mice. In L-DKO hearts, IRS1 and IRS2 proteins were reduced by 70 and 60%, respectively, compared with control (P < 0.05; Fig. 2*B* and Supplementary Fig. 2). There was reduced phosphorylation of Akt at S^{473} and phosphorylation of Foxo1 at S^{253} by at least 50% each (P < 0.05). There was a significant increase in p38 and JNK phosphorylation by 2.1- and 2.5-fold, respectively, whereas ERK1/2 phosphorylation was unchanged. These results suggest cardiac insulin resistance occurred in L-DKO mice, potentially through downregulation of IRS1 and IRS2.

Cardiac dysfunction in L-DKO mice. Echocardiographic analysis revealed that L-DKO hearts developed systolic cardiac dysfunction, as demonstrated by a 40% reduction in EF and a 20% reduction in FS, as well as diastolic dysfunction, as indicated by a 15% increase in isovolumic relaxation time and a 24% decrease in the E-to-A ratio, an indicator of early and late ventricular filling velocity (Fig. 2*C* and Table 1). The L-DKO heart had a reduction in ATP content by 20% compared with control (P < 0.05; Fig. 2*D*), demonstrated irregularly arranged cardiomyocytes (Fig. 2*E*), and exhibited mild fibrosis (Fig. 2*F*).

Expression of heart failure markers and energy metabolism genes in L-DKO hearts. In L-DKO hearts, the level of mRNAs encoding BNP and β-MHC was significantly increased by 1.5- and 3.8-fold, respectively, compared with control, whereas α-MHC was reduced. Expression of the fibrosis maker gene TGF-β1 and collagen I gene was mildly increased (Fig. 2*G*), whereas expression of IRS1 and IRS2 mRNA was not changed. L-DKO

fibrotic area under 500 μm^2 of sections. *P < 0.05 vs. control. *G*: Cardiac function of H-DKO and control mice at the age of 5 weeks was determined by echocardiography. Values are expressed as the mean ± SEM (n = 10). *P < 0.05 vs. control. *H*: Relative cardiac ATP level in H-DKO and control mice (n = 6). *P < 0.05 vs. control. *I*: Relative mRNA expression levels in the random-fed heart of H-DKO and control mice at the age of 5 weeks. Data are expressed as the mean ± SEM (n = 4). *P < 0.05 vs. control.
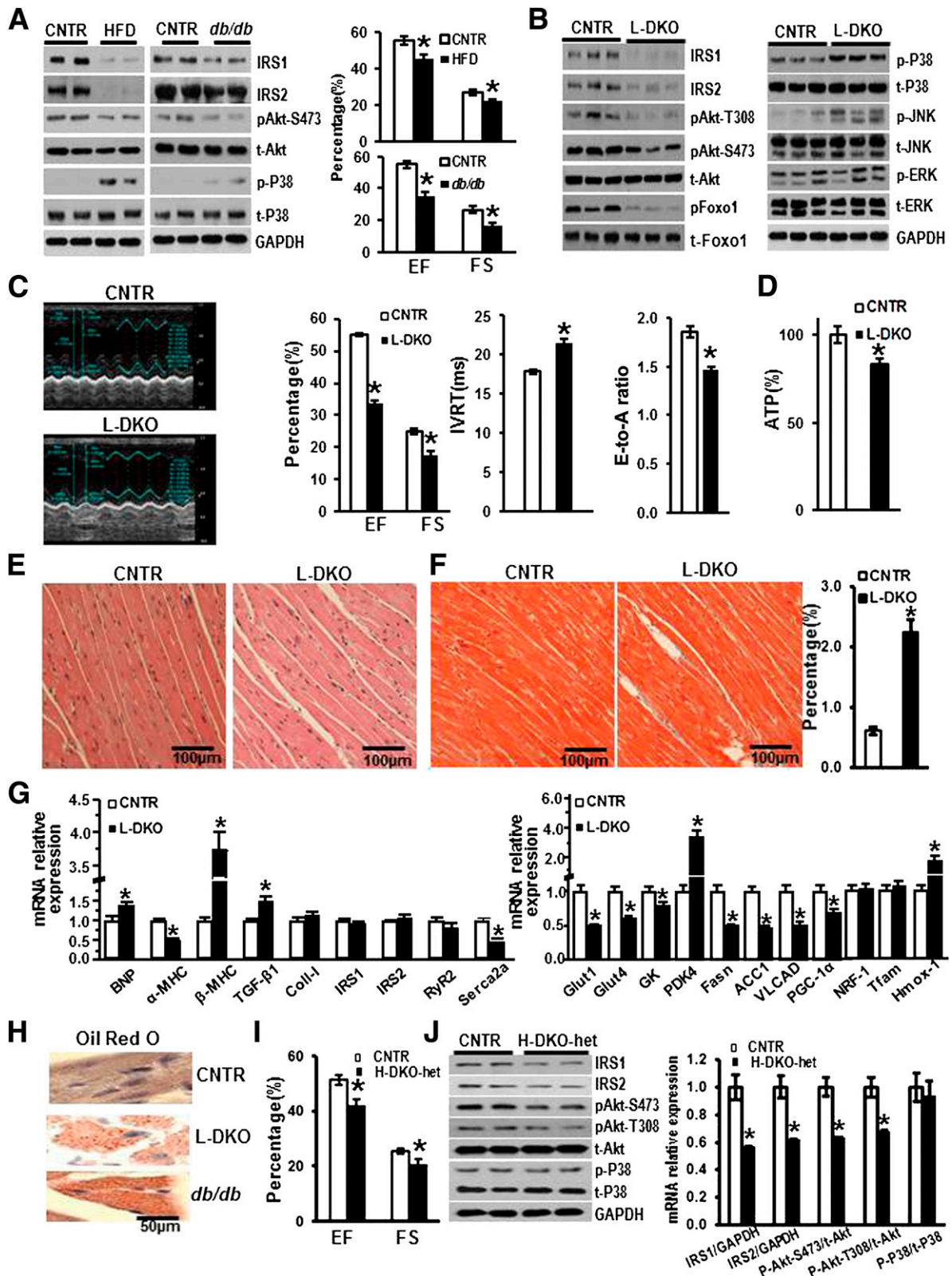
FIG. 2. Cardiac loss of IRS1 and IRS2 proteins in HFD, *db/db*, and L-DKO mice and cardiac dysfunction in L-DKO hearts compared with control (CNTR). Immunoblot analysis of insulin-signaling molecules in hearts and cardiac function of 5-month-old HFD, *db/db* mice, and control (*A*) and 6-month-old L-DKO mice (*B* and *C*) (*n* = 6–10). *P < 0.05 vs. control. All mice were in a random-fed state. Representative images of immunoblotting from two to three mice are shown. GAPDH, glyceraldehyde-3-phosphate dehydrogenase. *D*: Relative cardiac ATP content in the L-DKO and control mice (*n* = 6). *P < 0.05. Cardiac histology is shown by representative transverse section of left ventricle stained with hematoxylin and eosin (original magnification ×200) (*E*) and Masson Trichrome (original magnification ×200) (*F*), in which the percentage of the fibrotic area under 500 μm² of sections was presented. *P < 0.05 vs. control. *G*: Relative mRNA levels in the random-fed hearts of L-DKO and control mice. Data are expressed as the mean ± SEM (*n* = 4). *P < 0.05 vs. control. *H*: Oil red O staining of hearts from 6-month-old L-DKO, *db/db*, and control mice. *I*: Cardiac function of 6-month-old H-DKO-het mice (*n* = 6 per group). *P < 0.05 vs. control. *J*: Immunoblot analysis of insulin-signaling molecules in the random-fed hearts of H-DKO-het and control mice at random-fed state (*n* = 2–4 mice per group). *P < 0.05 vs. control.

FIG. 3. Chronic insulin (Ins) exposure reduces IRS1 and IRS2 and attenuates Akt→Foxo1 phosphorylation in cardiomyocytes. *A*: Immunoblot analysis of IRS, Akt, and Foxo1 phosphorylation after 100 nmol/L insulin treatment for 0.5, 3, and 24 h in NRVMs. *$P < 0.05$ vs. noninsulin treatment from three independent experiments. *B*: Detection of insulin sensitivity in NRVMs after chronic insulin treatment. Cells were treated with 100 nmol/L insulin for 24 h (Pre-Ins 24h) and washed with DMEM, followed by adding 100 nmol/L insulin for another 0.5 h, and cellular protein lysates were prepared for immunoblotting. Graphs indicate the relative expression levels of phosphorylation of Akt at S^{473} (p-Akt) and Foxo1 at S^{253} (p-Foxo1), which were normalized to total Akt and Foxo1 protein, respectively, from three different experiments. *$P < 0.05$ vs. noninsulin treatment. +$P < 0.05$ vs. 0.5 h insulin treatment in each group. *C*: Detection of insulin sensitivity after chronic high-glucose treatment in NRVMs. Cells were treated with 25 mmol/L glucose (HG), with or without 100 nmol/L insulin for 24 h, and then washed and treated with the same dose insulin for another 0.5 h, and cell protein lysates were prepared for immunoblotting. *$P < 0.05$ vs. noninsulin treatment; +$P < 0.05$ vs. HG plus 0.5 h

hearts exhibited mRNA levels of Glut1, Glut4, and GK that were reduced by 50, 40, and 15%, respectively, compared with control ($P < 0.05$). Lipid metabolism genes, such as Fasn, ACC1, and VLCAD, were decreased by 50% each, Pgc1α was reduced by 30% ($P < 0.05$), and PDK4 exhibited a 3.5-fold increase ($P < 0.05$) (Fig. 2G). L-DKO hearts exhibited markedly accumulated triglycerides, as revealed by Oil Red O staining, using *db/db* heart as control (Fig. 2H). Expression of Tfam and NRF1 was unchanged, Hmox-1 was increased by 2.2-fold, and expression of Serca2A was significantly decreased (Fig. 2G). Collectively, these results suggest that L-DKO hearts had reduced glucose and lipid utilization as well as impaired mitochondrial and calcium metabolism gene expression compared with control.

Downregulation of IRS1 and IRS2 results in cardiac dysfunction in H-DKO-het mice. We next determined whether a reduction of IRS1 and IRS2 is sufficient for cardiac dysfunction by analyzing H-DKO-het mice, which lack one allele each of IRS1 and IRS2. H-DKO-het mice survived normally. Echocardiographic analysis revealed that 6-month-old H-DKO-het mice developed cardiac dysfunction, as demonstrated by an 18% reduction in EF and a 19% reduction in FS (Fig. 2I). The H-DKO-het hearts displayed a 50% reduction in IRS1 and IRS2 protein levels, as well as Akt phosphorylation levels, compared with control (Fig. 2J).

Chronic insulin stimulation degrades IRS1 and IRS2 protein and causes insulin resistance in vitro. A major characteristic of L-DKO mice is hyperinsulinemia, accompanied by degradation of IRS1 and IRS2 in the heart. Thus, we determined whether insulin would cause myocardial insulin resistance by IRS protein regulation. First, we determined Akt→Foxo1 phosphorylation during different time courses of insulin stimulation of cardiomyocytes. NRVMs were treated with 100 nmol/L insulin for 0.5, 3, or 24 h, and cellular Akt and Foxo1 phosphorylation was determined using Western blot. Insulin treatment for 0.5 h robustly stimulated Akt and Foxo1 phosphorylation, whereas the effect of insulin was attenuated at 24 h (Fig. 3A). In parallel, protein levels of IRS1 and IRS2 were significantly decreased by 40 and 60%, respectively, after chronic insulin treatment (24 h), compared with non–insulin-treated cells (Fig. 3A).

Second, we determined whether chronic insulin exposure results in insulin resistance in cells. NRVMs were pretreated with 100 nmol/L insulin for 24 h (chronic stimulation), and the medium was changed and stimulated with the same dose of insulin for another 0.5 h (acute insulin stimulation). We found that chronic insulin treatment almost completely disrupted the effect of acute insulin stimulation on Akt and Foxo1 phosphorylation ($P < 0.05$; Fig. 3B), indicating that insulin itself causes insulin resistance by impairing Akt→Foxo1 phosphorylation, which is accompanied by a reduction in IRS1 and IRS2 protein. The effect of chronic insulin on attenuating Akt→Foxo1 phosphorylation was also observed in NRVMs cultured with 25 mmol/L glucose (high-glucose stimulation), in which high-glucose treatment did not significantly change IRS1 and IRS2 protein levels and only mildly altered the effect of acute insulin stimulation on Akt and Foxo1 phosphorylation ($P < 0.05$; Fig. 3C).

Finally, we determined whether the reduction in IRS1 or IRS2 contributed to chronic insulin resistance in cells.

NRVMs were infected with adenovirus expressing the gene encoding GFP, IRS1, or IRS2 and then treated with insulin for 24 h before acute insulin stimulation for 0.5 h. Western blot analysis indicated that impaired Akt→Foxo1 phosphorylation after chronic insulin exposure was largely prevented by overexpression of IRS1 or IRS2 (Fig. 3D). These results support our postulate that inhibition of IRS1 and IRS2 is a primary mediator causing insulin resistance during chronic insulin stimulation.

p38 mediates degradation of IRS1 and IRS2 after chronic insulin stimulation. In addition to Akt activation, acute insulin exposure (0.5 h) robustly induced ERK1/2 and slightly increased JNK phosphorylation, whereas chronic insulin exposure (24 h) persistently increased p38 phosphorylation (Fig. 4A). We next tested the hypothesis that activation of these kinases after chronic insulin exposure might be involved in the feedback degradation of IRS1 and IRS2, leading to myocardial insulin resistance. NRVMs were treated with the following kinase inhibitors: rapamycin (mTOR inhibitor), PD98059 (ERK1/2 inhibitor), and SB (p38 inhibitor) or SP (JNK inhibitor) for 0.5 h before 24 h of insulin stimulation, in which insulin-induced protein kinase phosphorylation/activation was completely blocked. We noted that SB had no effect on blocking p38 phosphorylation (Fig. 4B), which was consistent with a recent report that SB treatment effectively inhibited p38 activity without altering p38 phosphorylation in cardiomyocytes (24). Among these kinase inhibitors, the p38 inhibitor SB completely prevented chronic insulin-induced IRS1 and IRS2 degradation and rescued Akt→Foxo1 phosphorylation (Fig. 4C and D), suggesting that p38 activation is necessary for chronic insulin-induced IRS1 and IRS2 degradation and insulin resistance.

We next determined whether overexpression of p38 is sufficient for degrading IRS1 and IRS2 protein in cells. Overexpression of p38-WT, rather than p38-DN containing two amino acid mutations in the TGY motif to block phosphorylation at T and Y (TGY→AGF), reduced IRS1 and IRS2 protein levels by at least 80% in NRVMs, with or without 24 h of insulin treatment (Fig. 4E). Moreover, IRS1 and IRS2 protein and the basal level of Foxo1 phosphorylation were reduced by p38 in a dose-dependent manner (Fig. 4F). These results indicate that induction of p38 is necessary and sufficient for degrading IRS1 and IRS2 protein in insulin-signaling cascades.

p38 overexpression prevents the insulin effect on Akt→Foxo1 phosphorylation and metabolic gene expression in vitro. We next determined whether p38 overexpression causes insulin resistance by preventing insulin-induced Akt→Foxo1 phosphorylation and insulin-mediated gene expression in cells. NRVMs were infected with adenoviruses expressing GFP, p38-WT, and p38-DN and then treated with insulin for 0.5 h for cellular signaling analysis or 18 h for determination of insulin-regulated gene transcription. Compared with the non–insulin-treated control, p38 overexpression prevented the effect of 0.5 h of insulin stimulation on Akt→Foxo1 phosphorylation (Fig. 5A). Insulin treatment for 18 h stimulated expression of genes encoding α-MHC, Glut4, Fasn, and ACC1 by 1.8-, 1.4-, 2.5-, and 2.2-fold, respectively ($P < 0.05$), while inhibiting expression of genes encoding β-MHC and BNP by 50 and 70%,

---

insulin treatment. *D*: Overexpression of IRS1 or IRS2 rescued insulin sensitivity after chronic insulin treatment in NRVMs. Cells were infected with IRS1 or IRS2 adenovirus (Ad-IRS1 or Ad-IRS2, 75 MOI) for 8 h, starved 8 h with serum-free medium before insulin (Pre-Ins) 24 h, and then washed and treated with insulin for another 0.5 h. IRS, Akt, and Foxo1 phosphorylation were estimated by immunoblotting. +$P < 0.05$ vs. Ad-GFP with 0.5 h insulin treatment.
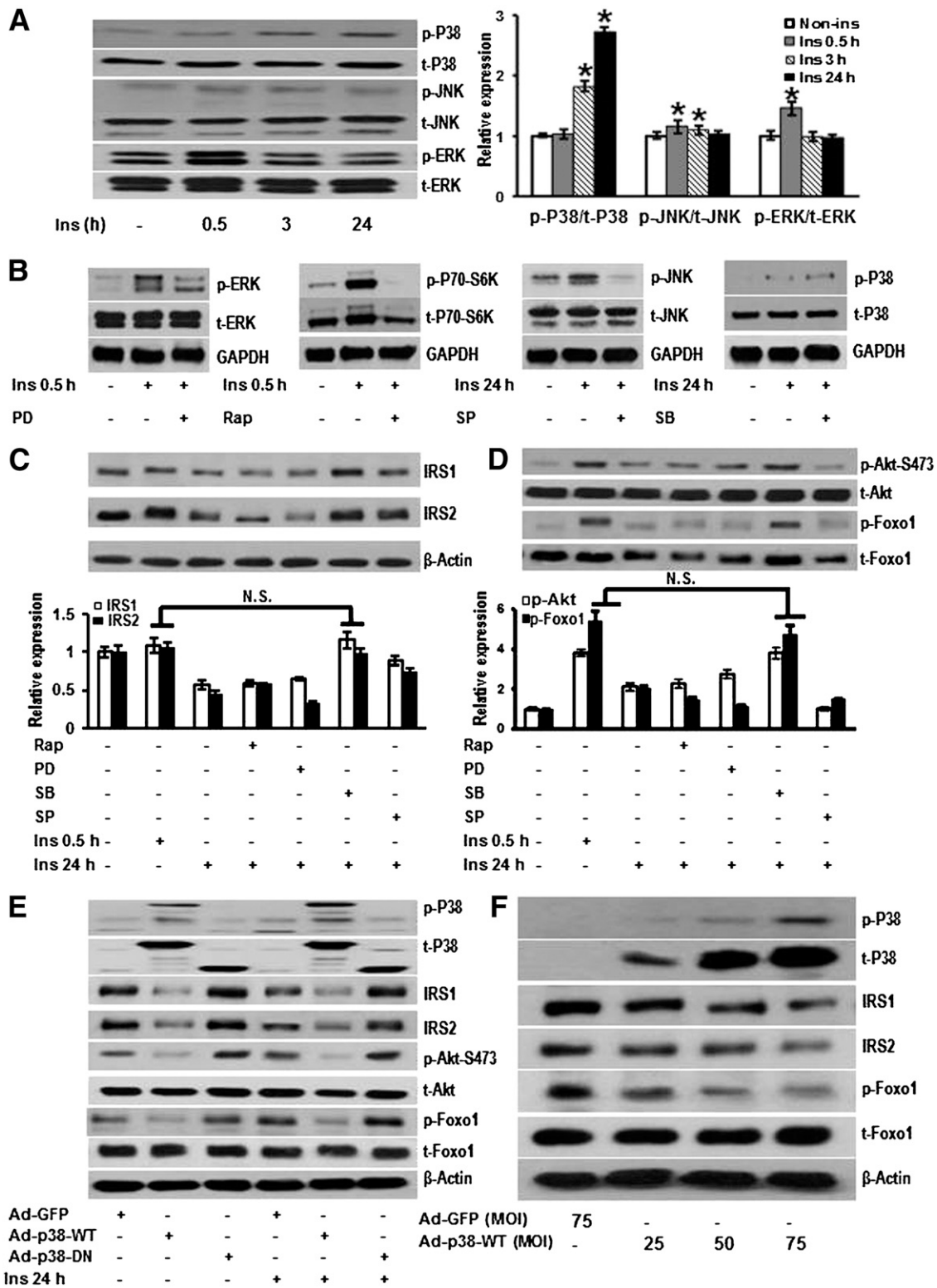
FIG. 4. p38 activation mediates chronic insulin-induced IRS1 and IRS2 degradation and is involved in myocardial insulin resistance in vitro. *A*: Immunoblot analysis of MAPK signaling components after 100 nmol/L insulin treatment for 0.5, 3, and 24 h in NRVMs. *$P < 0.05$ vs. noninsulin treatment. *B*: Effect of kinase inhibitors blocking phosphorylation of protein kinase: 20 μmol/L PD98059 (PD), 100 nmol/L rapamycin (Rap), 10 μmol/L SP600125 (SP), or 10 μmol/L SB203580 (SB) was added to NRVMs for 0.5 h before 100 nmol/L insulin treatment and cellular protein lysates prepared for immunoblotting. GAPDH, glyceraldehyde-3-phosphate dehydrogenase. p38 inhibitors prevented the degradation of IRS1 and IRS2 induced by chronic insulin treatment (*C*) and increased insulin sensitivity for Akt and Foxo1 phosphorylation (*D*). The kinase inhibitors rapamycin (100 nmol/L), PD98059 (20 μmol/L), SB203580 (10 μmol/L), or SP600125 (10 μmol/L) were separately added to serum-free medium for 0.5 h before insulin administration of NRVMs for 24 h. Cellular protein lysates were prepared for immunoblotting. Graphs indicate quantification of protein band density normalized to β-actin from at least 3 independent experiments. Data are expressed as the mean ± SEM. *E*: Overexpression of p38 degraded IRS1 and IRS2 in NRVMs. Cells were infected with adenovirus (75 MOI) expressing GFP, p38-WT, or p38-DN, and cellular protein lysates were prepared for immunoblotting. *F*: Dose-dependent effect of p38-WT on IRS1 and IRS2 degradation in NRVMs. Cells were infected with adenovirus expressing GFP or different amounts of adenovirus that express p38-WT. N.S., no significant difference.
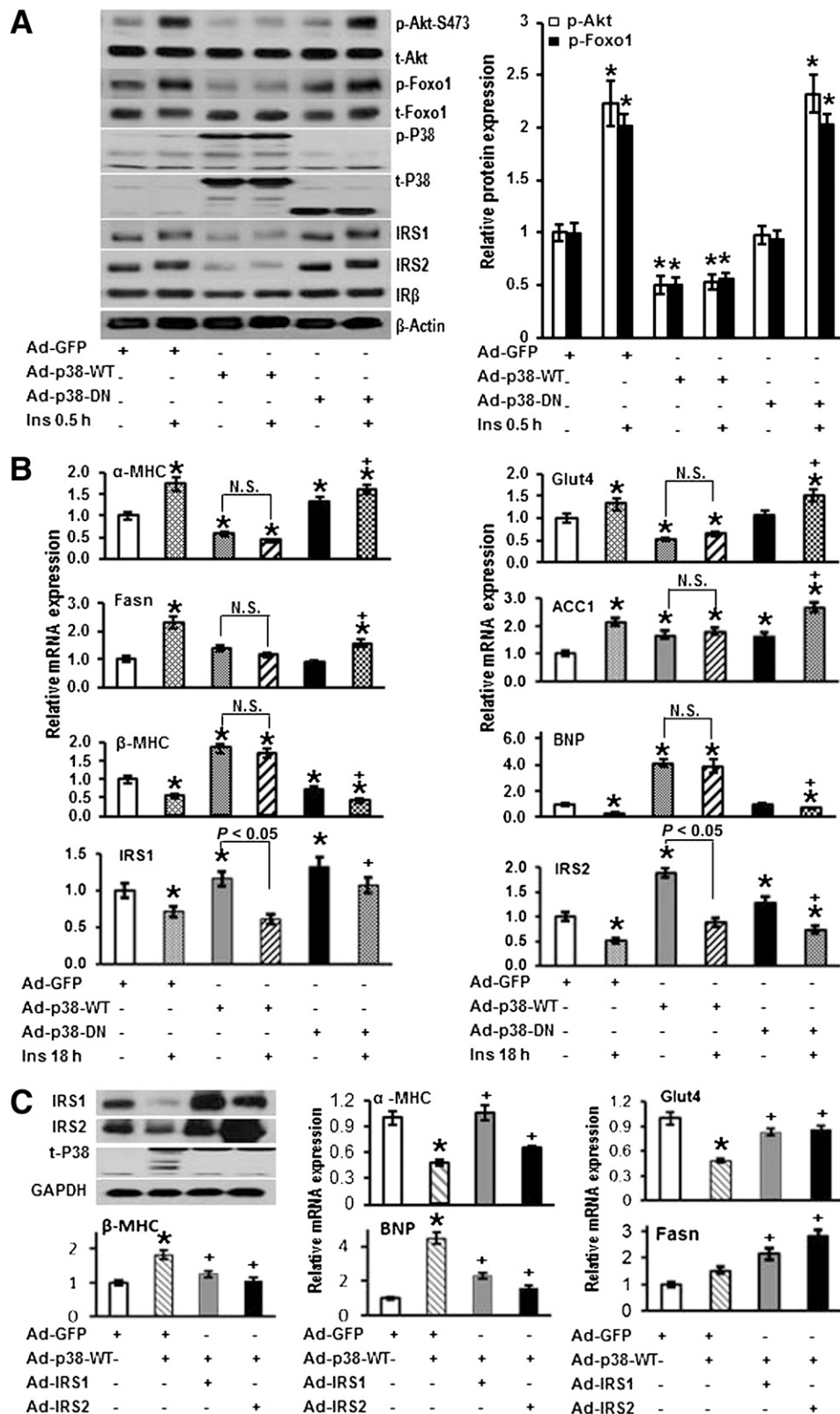
FIG. 5. p38 activation disrupts insulin-induced Akt and Foxo1 phosphorylation and insulin-regulated gene expression in cardiomyocytes. *A*: Overexpression of p38 blocked insulin-induced Akt and Foxo1 phosphorylation in NRVMs. Cells were transfected with adenovirus (Ad) expressing GFP, p38-WT, or p38-DN for 8 h and cultured in serum-free medium for another 8 h. Cells were then treated with 100 nmol/L insulin for 0.5 h, and cellular protein lysates were prepared for immunoblotting. *$P < 0.05$ vs. Ad-GFP treatment. *B*: Overexpression of p38-WT, rather than p38-DN, blocked insulin-stimulated or insulin-suppressed gene expression, as determined by real-time PCR in NRVMs. Cells were transfected with adenovirus expressing GFP, p38-WT, or p38-DN, followed by another 8 h of serum starvation. Cells were then treated with 100 nmol/L insulin for 18 h, and cellular RNA was prepared for real-time PCR analysis. Graphs indicate relative expression of genes encoding α-MHC, Glut4, Fasn, and ACC1 for insulin stimulation, or β-MHC, BNP, IRS1, and IRS2 for insulin inhibition. Data are expressed as the mean ± SEM from at least three independent experiments. *$P < 0.05$ vs. Ad-GFP; [+]$P < 0.05$ vs. Ad-p38-DN. *C*: Overexpression of IRS1 or IRS2 restored p38-WT–regulated

respectively ($P < 0.05$, Fig. 5B). These insulin-regulated effects were blocked by overexpression of p38-WT, rather than GFP or p38-DN, supporting the concept that p38 activation causes myocardial insulin resistance. Of note is that p38 overexpression did not block the effect of insulin on suppressing the transcriptional levels of IRS1 and IRS2 (Fig. 5B).

Overexpression of IRS1 or IRS2 prevents p38-induced heart failure and metabolic gene expression. To determine if maintaining IRS expression is sufficient to reverse gene expression changes induced by p38 activation in cultured cells, we co-overexpressed p38, together with control GFP, IRS1, or IRS2, and analyzed gene transcriptional profiles. The results indicated that overexpression of IRS1 or IRS2 completely or partially rescued β-MHC, α-MHC, and BNP (heart failure genes) and metabolic gene expression such as Glut4 (Fig. 5C).

Chronic insulin treatment prevents the effect of insulin on metabolic gene expression and promotes IRS1 phosphorylation at Ser 636 in vitro. Similar to p38 overexpression, 24 h of chronic insulin exposure prevented the effect of 18 h of insulin on expression of genes encoding α-MHC, Glut-4, Fasn, and ACC1 (stimulation) and β-MHC and BNP (inhibition). The insulin inhibition on IRS1 and IRS2 gene transcription was maintained after the chronic insulin exposure (Fig. 6A).

IRS1 and IRS2 serine or threonine phosphorylation is believed to mediate IRS degradation, ubiquitination, and insulin resistance (25). Thus, we determined the insulin effect on IRS1 serine phosphorylation at S^{636} and S^{612}, both of which mediate IRS1 degradation or inhibition (26,27). Insulin treatment for 24 h or p38 overexpression increased phosphorylation at both residues, and p38-DN expression also increased IRS1-S^{612} phosphorylation (Fig. 6B and C), suggesting that IRS1-S^{636} may participate in IRS1 inhibition and degradation. We further determined whether the 26S proteasome-activated ubiquitination pathway mediates p38- or chronic insulin-induced IRS1 or IRS2 degradation. Treatment with MG132, a 26S proteasome inhibitor, prevented chronic insulin- or p38-WT–induced degradation of IRS2, rather than IRS1 (Fig. 6D and E). Of note is that MG132 induced IRS1 degradation, the mechanism of which is unknown. These results suggest that IRS1 and IRS2 degradation is mediated by distinct mechanisms in which IRS2 is involved in the 26S proteasome pathway and IRS1 is involved in S^{636} phosphorylation.

Finally, we determined whether insulin degrades IRS proteins in a dose-dependent manner. Insulin treatment for 24 h resulted in reduced IRS1 and IRS2 in a dose-dependent manner, in which IRS2 had a higher sensitivity for reduction than IRS1 after insulin treatment (Fig. 6F).

DISCUSSION

In this study, we present three important findings: First, IRS1 and IRS2 have key roles in regulating cardiac homeostasis, energy metabolism, and function. A loss of IRS1 and IRS2 in the heart (H-DKO mice) increases apoptosis; decreases ventricular mass; increases interstitial fibrosis; diminishes myocardial Akt→Foxo1 phosphorylation; impairs cardiac metabolism, calcium handling, and myosin gene expression; and reduces cardiac ATP content, with sudden death of animals beginning at 6 to 8 weeks of age.

Second, a 50% reduction in cardiac IRS1 and IRS2 is sufficient for induction of cardiac dysfunction, and downregulation of both genes occurs in insulin-resistant or type 2 diabetic mouse models (HFD, *db/db*, and L-DKO mice).

Third, chronic insulin exposure promotes IRS1 and IRS2 degradation, resulting in myocardial insulin resistance, in which p38 activation is necessary and sufficient for the effect of chronic insulin action.

Given that the Akt and MAP kinase pathways are both important for cardiac biology and function and are activated by many stimuli, including mechanical stretch, growth factors, and hormones through a variety of receptor tyrosine kinases or G-protein–coupled receptors (28), it is unclear which endogenous upstream mediators govern the downstream effectors for Akt and MAPK activation (29). In this study, we used H-DKO mice to provide evidence demonstrating that IRS1 and IRS2 are major mediators for the endogenous cardiac Akt→Foxo1 signaling cascade. Importantly, the RAS→MAPK cascades are not dependent on IRS1 and IRS2, suggesting that other IR-associated proteins may be involved in the activation of MAPKs. Thus, we expect that deactivation of Akt resulting from inactivation of PDK1 and PDK2 in H-DKO hearts may mediate the heart failure observed. In fact, cardiac inactivation of PDK1 is sufficient for the development of dilated heart failure with apoptosis and fibrosis (30,31), similar to the phenotype observed in H-DKO hearts. Akt is required for cardiac growth, metabolism, and survival (32), and targets of Akt include p70S6K (protein synthesis), glut4 (glucose transport), and Foxo1 (gene expression) (9,33,34).

Cardiac inactivation of Akt after the loss of IRS1 and IRS2 may serve as a central mechanism for the induction of heart failure, which involves multiple mechanisms (Fig. 7A):

1) Akt inactivation promotes cardiac apoptosis, at least by Foxo1 activation, that promotes cell death (35). The incidence of myocardial apoptosis in the H-DKO heart is relatively small (1%), but a minimal increase can be of considerable biological importance on myocardial homeostasis and morphology. Indeed, Foxo1 deficiency in H-DKO mice prevented early death and cardiac dysfunction (Y.Q. and S.G., unpublished data).

2) Akt inactivation activates Foxo1 resulting in heme deficiency, limiting mitochondrial cofactor biosynthesis and ATP production, as we observed in liver lacking both IRS1 and IRS2 (20). Heme is an essential component for mitochondrial complex III and IV and it is controlled by Hmox-1, a Foxo1 target gene promoting heme degradation (20).

3) PI3K→Akt activation is required for proper calcium handling because blocking PI3K or Akt markedly decreases intracellular calcium transients essential for cardiac contraction (36), which may also involve RyR2 and Serca2A gene expression and regulation.

4) PI3K→Akt activation is required for controlling MHC plasticity and motor gene expression, which is required for

---

transcriptional levels of heart failure and metabolic genes in cells. NRVMs were transfected with 50 MOI p38WT and 50 MOI adenovirus expressing GFP, IRS1, or IRS2 for 8 h, followed by another 8 h in serum-rich DMEM medium. The protein or RNA was prepared for Western blot or real-time PCR, respectively. Representative data from Western-blot and quantitative PCR are shown. *$P < 0.05$ vs. Ad-GFP; +$P < 0.05$ vs. Ad-p38WT. N.S., no significant difference.
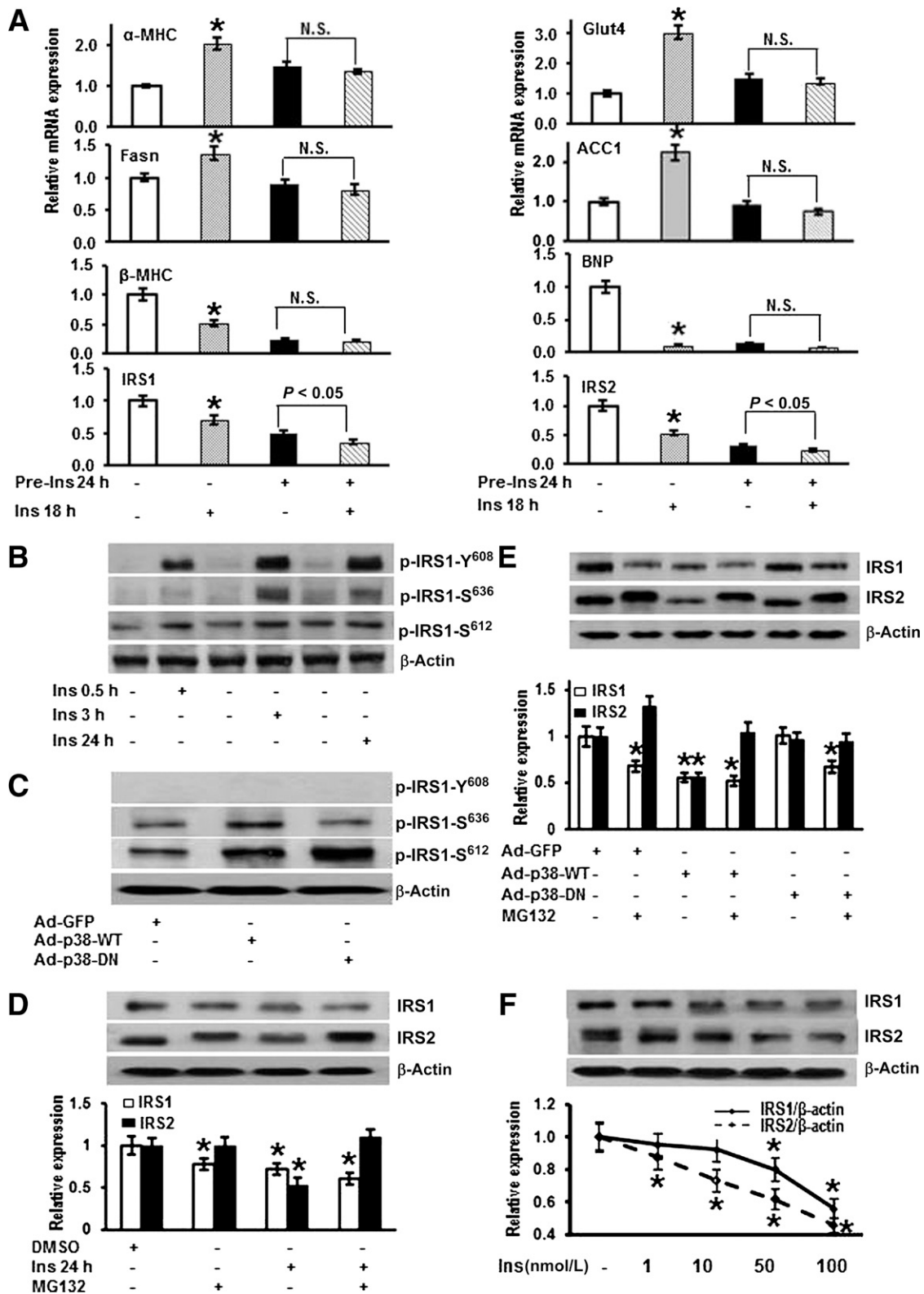
FIG. 6. Chronic insulin exposure blocks the effect of insulin on metabolic gene expression and induces IRS1-S636 phosphorylation and IRS2 ubiquitylation in cardiomyocytes. *A*: Chronic insulin exposure disrupted insulin-induced gene expression in cells. NRVMs were treated with 100 nmol/L insulin for 24 h (Pre-Ins 24 h) and then washed and treated with or without 100 nmol/L insulin for another 18 h, before harvesting of cellular RNA for real-time PCR determination. Graphs indicate relative expression of genes. Data are expressed as the mean ± SEM from at least three different experiments. *$P < 0.05$ vs. noninsulin treatment. *B*: Insulin induced phosphorylation of IRS1 at S^{636} and S^{612} in NRVMs. Cells were treated with 100 nmol/L insulin for 0.5, 3, and 24 h, and S^{636}, S^{612}, and Y^{608} of IRS1 were determined by immunoblotting. *C*: p38-WT and p38-DN differentially induced IRS1 serine phosphorylation at S^{636} and S^{612} in cells. NRVMs were infected with adenovirus as indicated (75 MOI), and cellular protein lysates were prepared for immunoblotting. *D* and *E*: Chronic insulin or p38 overexpression mediated IRS2 degradation in a 26S proteasome-dependent manner in cells. NRVMs were treated with 10 μmol/L MG132 for 0.5 h before 100 nmol/L insulin treatment for 24 h, and cellular proteins were then prepared for immunoblotting. *E*: For adenovirus infection, the cells were treated with MG132 for 0.5 h, and then
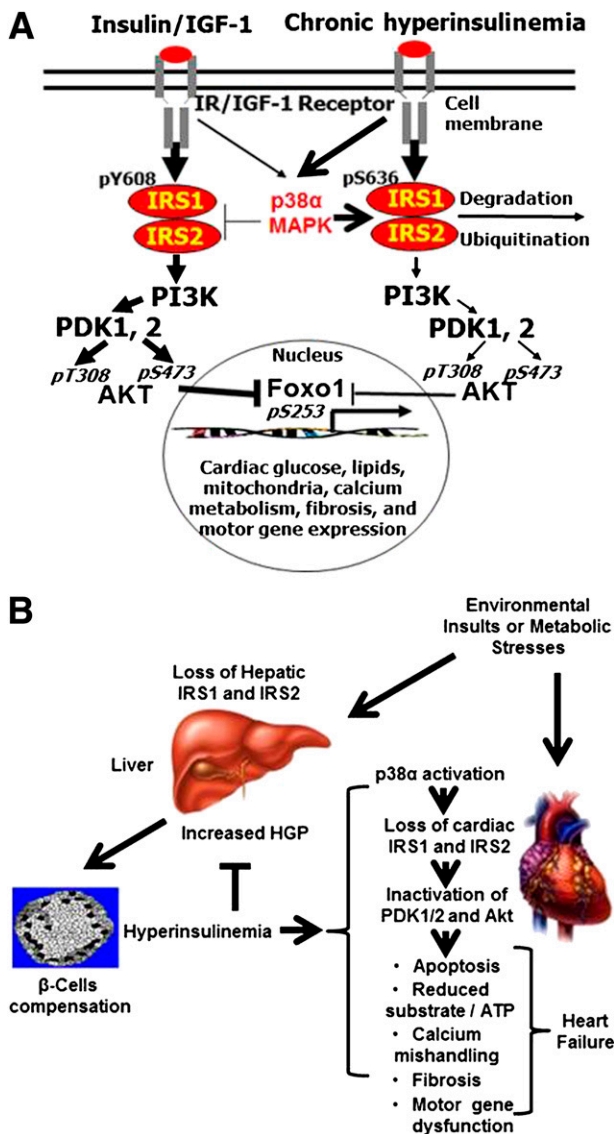
FIG. 7. A: Schematic diagram represents the role of acute and chronic insulin in regulating IRS1 and IRS2 via p38 MAPK. B: Downregulation of IRS1 and IRS2 by metabolic stresses and/or environmental insults triggers insulin resistance in the liver and promotes insulin secretion from pancreatic β-cells. Activation of p38 in the heart by hyperinsulinemia or other metabolic stresses promotes IRS1 and IRS2 degradation and dysregulates cardiac glucose and lipid metabolism, mitochondrial biogenesis, calcium-handling, fibrosis, and motor gene expression, resulting in heart failure. HGP, hepatic glucose production.

normal cardiac contractility. This is controlled by Foxo1 that promotes β-MHC gene expression (Q.Z. and S.G., unpublished data).

5) Inactivation of PDK1 promotes cardiac fibrosis, suggesting that unknown factors released from the myocardium after loss of IRS1 and IRS2 and Akt inactivation may influence cell communications between myocytes and nonmyocytes, resulting in interstitial fibrosis and cardiac failure.

IRS1 and IRS2 also mediate the effect of IGF-1, which can activate PI-3K and MAPK pathways through the IGF-1 receptor. Mice deficient in cardiac and skeletal muscle in both insulin and the IGF-1 receptor, rather than each alone, died of heart failure in the first month of life with cardiac Akt inactivation (37), suggesting that insulin or IGF-1 is cardioprotective for survival. Activation of Foxo1, resulting from inactivation of Akt, may contribute to heart failure because overexpression of a constitutive active Foxo1 in the heart resulted in embryonic lethality at 10.5 days of gestation, with overt heart failure in mice (13), whereas inactivation of Foxo1 in the heart prevented heart failure in HFD-induced insulin-resistant mice (12). Conversely, MAPKs have different roles in cardiac biology. For example, loss of ERK1/2 had no effect on the cardiac growth responses, but overexpression of ERK promoted cardiac hypertrophy in mice (38), loss of cardiac p38 promoted cardiac hypertrophy (39), and cardiac JNK inactivation inhibited cardiac apoptosis and activation inhibited hypertrophic responses in pressure overload (40). Collectively, cardiac PI-3K→Akt→Foxo1 and MAPKs activation have differential roles in the heart, but the IRS1- and IRS2-associated Akt activation is essential for cardiac growth, survival, and function.

In our cell-based studies, chronic high glucose exposure did not significantly alter the IRS1 or IRS2 protein level and minimally reduced insulin-stimulated Akt→Foxo1 phosphorylation. However, chronic insulin exposure results in insulin resistance by decreasing IRS1 and IRS2 at the mRNA and protein levels. Insulin resistance is implicated in the pathogenesis of type 2 diabetes, and insulin serves as an inducer of insulin resistance in liver and adipose tissue (41). In the heart, hyperinsulinemic exposure also exacerbates cardiac systolic dysfunction, caused by pressure overload in mice (42). Diabetic cardiomyopathy is directly related to hyperglycemia, independent of hypertension or coronary atherosclerosis (43), and hyperglycemia is currently believed to promote production of reactive oxygen species, advanced glycation end products, and metabolic perturbations that result in increased glucose toxicity and myocardial injury and apoptosis (21,44). Hyperglycemia and hyperinsulinemia may cause cardiac dysfunction through different mechanisms, in which loss of IRS1 and IRS2 by chronic insulin stimulation may provide a fundamental mechanism for heart failure in insulin resistance and type 2 diabetes. Of note is that the presence of IRS1 or IRS2 alone maintained cardiac function to support animal survival (19).

p38 phosphorylation increases in the heart of insulin-resistant and diabetic mice (HFD, *db/db*, and L-DKO mice) and is closely associated with downregulation of IRS1 and IRS2 protein levels and Akt inactivation. Recent studies demonstrated that the HFD dramatically increased the death rate of animals, secondary to heart failure resulting from Akt inactivation (12). Importantly, p38 activation is implicated in a wide spectrum of cardiac pathologies, including myocardial infarction, inflammation (45), and metabolic stress (46), in which some insults may be secondary to IRS1 and IRS2 degradation in response to mechanical and metabolic stresses (47). Administration of p38 chemical inhibitors prevented diabetes and pressure overload–induced cardiac dysfunction in

mice (46,48), and we expect that p38 inhibition in L-DKO mice would also improve the cardiac dysfunction.

p38 mediates the effect of chronic insulin on promoting insulin resistance by suppressing IRS1 and IRS2. p38 and insulin both promoted IRS2 degradation via a 26S proteasome–dependent ubiquitination pathway, whereas IRS1 degradation in cardiomyocytes was independent of this pathway (Fig. 7A). IRS1-S^{612} and -S^{636} phosphorylation reduced PI-3K in skeletal muscle of patients with type 2 diabetes (49), and S^{636} phosphorylation was also increased by the inflammatory factor tumor necrosis factor-α (26,50). In our studies, p38-DN–induced S^{612} phosphorylation did not block insulin action, an observation that conceptually supports IRS1-S^{636} phosphorylation as important in IRS1 degradation; but the coupling mechanism of IRS1 degradation and S^{636} phosphorylation will necessitate further investigation. Of note, whether p38 can directly interact with IRS1 to phosphorylate S^{636} has not been validated, because p38 also targets other intracellular protein kinases, such as cAMP-dependent protein kinase, for metabolic regulation (51). Regardless, our data suggest that p38 activation in the myocardium triggers distinct regulatory mechanisms for IRS1 and IRS2 protein degradation, independent of gene transcriptional regulation.

In conclusion, our data indicate IRS1 and IRS2 have major roles in the control of cardiac homeostasis, metabolism, and function, while suppressing cardiac IRS1 and IRS2 may serve as a fundamental mechanism for induction of heart failure (Fig. 7B). We believe that sensitizing myocardial Akt→Foxo1 signaling by integrating insulin therapy and blocking the p38→IRS1/2 signaling cascade will provide new insight in the treatment of heart failure during insulin resistance, type 2 diabetes, or other chronic physiologic stresses.

REFERENCES

1. Roger VL, Go AS, Lloyd-Jones DM, et al.; American Heart Association Statistics Committee and Stroke Statistics Subcommittee. Heart disease and stroke statistics—2011 update: a report from the American Heart Association. Circulation 2011;123:e18–e209

2. Wilson C. Diabetes: ACCORD: 5-year outcomes of intensive glycemic control. Nat Rev Endocrinol 2011;7:314

3. Randle PJ, Garland PB, Hales CN, Newsholme EA. The glucose fatty-acid cycle. Its role in insulin sensitivity and the metabolic disturbances of diabetes mellitus. Lancet 1963;1:785–789

4. White MF. Insulin signaling in health and disease. Science 2003;302:1710–1711

5. Guo S, Copps KD, Dong X, et al. The Irs1 branch of the insulin signaling cascade plays a dominant role in hepatic nutrient homeostasis. Mol Cell Biol 2009;29:5070–5083

6. Guo S. Molecular basis of insulin resistance: the role of IRS and Foxo1 in the control of diabetes mellitus and its complications. Drug Discov Today Dis Mech 2013;10:e27–e33

7. Alessi DR, James SR, Downes CP, et al. Characterization of a 3-phosphoinositide-dependent protein kinase which phosphorylates and activates protein kinase Balpha. Curr Biol 1997;7:261–269

8. Sarbassov DD, Guertin DA, Ali SM, Sabatini DM. Phosphorylation and regulation of Akt/PKB by the rictor-mTOR complex. Science 2005;307:1098–1101

9. Guo S, Rena G, Cichy S, He X, Cohen P, Unterman T. Phosphorylation of serine 256 by protein kinase B disrupts transactivation by FKHR and mediates effects of insulin on insulin-like growth factor-binding protein-1 promoter activity through a conserved insulin response sequence. J Biol Chem 1999;274:17184–17192

10. Zhang K, Li L, Qi Y, et al. Hepatic suppression of Foxo1 and Foxo3 causes hypoglycemia and hyperlipidemia in mice. Endocrinology 2012;153:631–646

11. Hannenhalli S, Putt ME, Gilmore JM, et al. Transcriptional genomics associates FOX transcription factors with human heart failure. Circulation 2006;114:1269–1276

12. Battiprolu PK, Hojayev B, Jiang N, et al. Metabolic stress-induced activation of FoxO1 triggers diabetic cardiomyopathy in mice. J Clin Invest 2012;122:1109–1118

13. Evans-Anderson HJ, Alfieri CM, Yutzey KE. Regulation of cardiomyocyte proliferation and myocardial growth during development by FOXO transcription factors. Circ Res 2008;102:686–694

14. Shiraishi I, Melendez J, Ahn Y, et al. Nuclear targeting of Akt enhances kinase activity and survival of cardiomyocytes. Circ Res 2004;94:884–891

15. Guo S, Dunn SL, White MF. The reciprocal stability of FOXO1 and IRS2 creates a regulatory circuit that controls insulin signaling. Mol Endocrinol 2006;20:3389–3399

16. Araki E, Lipes MA, Patti ME, et al. Alternative pathway of insulin signalling in mice with targeted disruption of the IRS-1 gene. Nature 1994;372:186–190

17. Withers DJ, Gutierrez JS, Towery H, et al. Disruption of IRS-2 causes type 2 diabetes in mice. Nature 1998;391:900–904

18. Dong XC, Copps KD, Guo S, et al. Inactivation of hepatic Foxo1 by insulin signaling is required for adaptive nutrient homeostasis and endocrine growth regulation. Cell Metab 2008;8:65–76

19. Long YC, Cheng Z, Copps KD, White MF. Insulin receptor substrates Irs1 and Irs2 coordinate skeletal muscle growth and metabolism via the Akt and AMPK pathways. Mol Cell Biol 2011;31:430–441

20. Cheng Z, Guo S, Copps K, et al. Foxo1 integrates insulin signaling with mitochondrial function in the liver. Nat Med 2009;15:1307–1311

21. Nizamutdinova IT, Guleria RS, Singh AB, Kendall JA Jr, Baker KM, Pan J. Retinoic acid protects cardiomyocytes from high glucose-induced apoptosis through inhibition of NF-κB signaling pathway. J Cell Physiol 2013;228:380–392

22. Furuyama T, Kitayama K, Yamashita H, Mori N. Forkhead transcription factor FOXO1 (FKHR)-dependent induction of PDK4 gene expression in skeletal muscle during energy deprivation. Biochem J 2003;375:365–371

23. Buchanan J, Mazumder PK, Hu P, et al. Reduced cardiac efficiency and altered substrate metabolism precedes the onset of hyperglycemia and contractile dysfunction in two mouse models of insulin resistance and obesity. Endocrinology 2005;146:5341–5349

24. Auger-Messier M, Accornero F, Goonasekera SA, et al. Unrestrained p38 MAPK activation in Dusp1/4 double-null mice induces cardiomyopathy. Circ Res 2013;112:48–56

25. Copps KD, White MF. Regulation of insulin sensitivity by serine/threonine phosphorylation of insulin receptor substrate proteins IRS1 and IRS2. Diabetologia 2012;55:2565–2582

26. Bouzakri K, Roques M, Gual P, et al. Reduced activation of phosphatidylinositol-3 kinase and increased serine 636 phosphorylation of insulin receptor substrate-1 in primary culture of skeletal muscle cells from patients with type 2 diabetes. Diabetes 2003;52:1319–1325

27. Hemi R, Yochananov Y, Barhod E, et al. p38 mitogen-activated protein kinase-dependent transactivation of ErbB receptor family: a novel common

mechanism for stress-induced IRS-1 serine phosphorylation and insulin resistance. Diabetes 2011;60:1134–1145

28. Sussman MA, Völkers M, Fischer K, et al. Myocardial AKT: the omnipresent nexus. Physiol Rev 2011;91:1023–1070

29. Liew CC, Dzau VJ. Molecular genetics and genomics of heart failure. Nat Rev Genet 2004;5:811–825

30. Mora A, Davies AM, Bertrand L, et al. Deficiency of PDK1 in cardiac muscle results in heart failure and increased sensitivity to hypoxia. EMBO J 2003;22:4666–4676

31. Ito K, Akazawa H, Tamagawa M, et al. PDK1 coordinates survival pathways and beta-adrenergic response in the heart. Proc Natl Acad Sci U S A 2009;106:8689–8694

32. DeBosch B, Treskov I, Lupu TS, et al. Akt1 is required for physiological cardiac growth. Circulation 2006;113:2097–2104

33. McMullen JR, Shioi T, Zhang L, et al. Deletion of ribosomal S6 kinases does not attenuate pathological, physiological, or insulin-like growth factor 1 receptor-phosphoinositide 3-kinase-induced cardiac hypertrophy. Mol Cell Biol 2004;24:6231–6240

34. Abel ED, Kaulbach HC, Tian R, et al. Cardiac hypertrophy with preserved contractile function after selective deletion of GLUT4 from the heart. J Clin Invest 1999;104:1703–1714

35. Modur V, Nagarajan R, Evers BM, Milbrandt J. FOXO proteins regulate tumor necrosis factor-related apoptosis inducing ligand expression. Implications for PTEN mutation in prostate cancer. J Biol Chem 2002;277: 47928–47937

36. Graves BM, Simerly T, Li C, Williams DL, Wondergem R. Phosphoinositide-3-kinase/akt - dependent signaling is required for maintenance of [Ca(2+)] (i), I(Ca), and Ca(2+) transients in HL-1 cardiomyocytes. J Biomed Sci 2012;19:59

37. Laustsen PG, Russell SJ, Cui L, et al. Essential role of insulin and insulin-like growth factor 1 receptor signaling in cardiac development and function. Mol Cell Biol 2007;27:1649–1664

38. Purcell NH, Wilkins BJ, York A, et al. Genetic inhibition of cardiac ERK1/2 promotes stress-induced apoptosis and heart failure but has no effect on hypertrophy in vivo. Proc Natl Acad Sci U S A 2007;104:14074–14079

39. Braz JC, Bueno OF, Liang Q, et al. Targeted inhibition of p38 MAPK promotes hypertrophic cardiomyopathy through upregulation of calcineurin-NFAT signaling. J Clin Invest 2003;111:1475–1486

40. Kaiser RA, Liang Q, Bueno O, et al. Genetic inhibition or activation of JNK1/2 protects the myocardium from ischemia-reperfusion-induced cell death in vivo. J Biol Chem 2005;280:32602–32608

41. Cao W, Liu HY, Hong T, Liu Z. Excess exposure to insulin may be the primary cause of insulin resistance. Am J Physiol Endocrinol Metab 2010; 298:E372

42. Shimizu I, Minamino T, Toko H, et al. Excessive cardiac insulin signaling exacerbates systolic dysfunction induced by pressure overload in rodents. J Clin Invest 2010;120:1506–1514

43. Rubler S, Dlugash J, Yuceoglu YZ, Kumral T, Branwood AW, Grishman A. New type of cardiomyopathy associated with diabetic glomerulosclerosis. Am J Cardiol 1972;30:595–602

44. Singh VP, Le B, Khode R, Baker KM, Kumar R. Intracellular angiotensin II production in diabetic rats is correlated with cardiomyocyte apoptosis, oxidative stress, and cardiac fibrosis. Diabetes 2008;57:3297–3306

45. Li M, Georgakopoulos D, Lu G, et al. p38 MAP kinase mediates inflammatory cytokine induction in cardiomyocytes and extracellular matrix remodeling in heart. Circulation 2005;111:2494–2502

46. Chai W, Wu Y, Li G, Cao W, Yang Z, Liu Z. Activation of p38 mitogen-activated protein kinase abolishes insulin-mediated myocardial protection against ischemia-reperfusion injury. Am J Physiol Endocrinol Metab 2008; 294:E183–E189

47. Friehs I, Cao-Danh H, Nathan M, McGowan FX, del Nido PJ. Impaired insulin-signaling in hypertrophied hearts contributes to ischemic injury. Biochem Biophys Res Commun 2005;331:15–22

48. Westermann D, Rutschow S, Van Linthout S, et al. Inhibition of p38 mitogen-activated protein kinase attenuates left ventricular dysfunction by mediating pro-inflammatory cardiac cytokine levels in a mouse model of diabetes mellitus. Diabetologia 2006;49:2507–2513

49. Mothe I, Van Obberghen E. Phosphorylation of insulin receptor substrate-1 on multiple serine residues, 612, 632, 662, and 731, modulates insulin action. J Biol Chem 1996;271:11222–11227

50. Plomgaard P, Bouzakri K, Krogh-Madsen R, Mittendorfer B, Zierath JR, Pedersen BK. Tumor necrosis factor-alpha induces skeletal muscle insulin resistance in healthy human subjects via inhibition of Akt substrate 160 phosphorylation. Diabetes 2005;54:2939–2945

51. Cao W, Daniel KW, Robidoux J, et al. p38 mitogen-activated protein kinase is the central regulator of cyclic AMP-dependent transcription of the brown fat uncoupling protein 1 gene. Mol Cell Biol 2004;24:3057–3067